J Mater Sci (2021) 56:16010–16027

Energy materials

Performance and morphology of centrifugally spun Co_3O_4/C composite fibers for anode materials in lithium-ion batteries

Jonathan Ayala[1], Daniel Ramirez[2], Jason C. Myers[3], Timothy P. Lodge[4], Jason Parsons[2], and Mataz Alcoutlabi[1,*]

[1] Department of Mechanical Engineering, University of Texas, Rio Grande Valley, 1201 W University Dr, Edinburg, TX 78539, USA
[2] Department of Chemistry, University of Texas, Rio Grande Valley, 1 W University Blvd, Brownsville, TX 78521, USA
[3] College of Science and Engineering, 55 Shepherd Labs, University of Minnesota, Minneapolis, MN 55455-0431, USA
[4] Department of Chemical Engineering and Materials Science and Department of Chemistry, University of Minnesota, Minneapolis, MN 55455-0431, USA

Received: 3 March 2021
Accepted: 24 June 2021
Published online: 9 July 2021

ABSTRACT

Centrifugally spun polyacrylonitrile (PAN) microfibers surface-coated with Co_3O_4 nanoparticles were prepared as precursors to produce coated Co_3O_4 carbon-fiber (CCF) composites for lithium-ion battery anodes. The Co_3O_4/C composite-fiber anodes were obtained after the stabilization of surface-coated Co_3O_4/PAN fibers at 200 °C for four hours, and subsequent carbonization at 600 °C for 6 hours. The electrochemical performance of the Co_3O_4/C composite-fiber anode with different active material loading was evaluated by using galvanostatic charge/discharge, rate performance, cyclic voltammetry, and electrochemical impedance spectroscopy experiments. The CCF anode delivered a specific charge capacity of 632 and 420 mAh g^{-1} after 100 cycles at 100 and 200 mA g^{-1}, respectively, and exhibited good rate capability. An improved electrochemical performance of the CCF was observed compared to the carbon-fiber (CF) anode (300 mAh g^{-1}), which was attributed to the interaction between CFs and Co_3O_4 nanoparticles. The synthesis method presented in this work can provide an effective avenue for the fabrication of surface coated-fiber materials, including free-standing anode materials for lithium-ion batteries with increased specific capacity and improved electrochemical performance compared to carbon-fiber electrodes.

Handling Editor: Mark Bissett.

Address correspondence to E-mail: mataz.alcoutlabi@utrgv.edu

https://doi.org/10.1007/s10853-021-06285-3

GRAPHICAL ABSTRACT

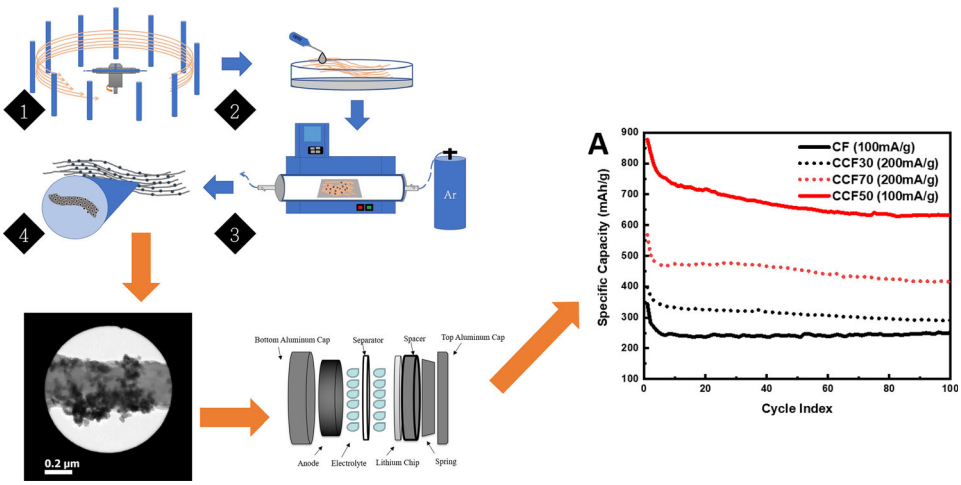

Introduction

Nanofibers can facilitate unique nanostructured materials for different applications. The characteristically high aspect ratio as well as mass production methods such as centrifugal spinning led to nanofibers becoming a main focus area of research in the field of nano-/microstructured materials, including biosensors, air filtration, and antibacterial applications [1–3]. In addition, a large portion of nanofiber-based research has been dedicated to energy storage applications [4–8].

Rechargeable lithium-ion batteries (LIBs) currently are ascendant in technological expansion for energy storage. Modern devices require increased electrochemical performance, in terms of both power and efficiency, as well as superior physical properties such as low density and electrode-material flexibility to enable a wide array of designs. While electrode technology has been investigated for decades, novel electrode chemistries are still being sought.

Composite nanofibers have attracted attention in recent years as electrode materials for LIBs and sodium-ion batteries (SIBs) due to their low cost and good capacity. Electrospinning has been the most prominent method of preparing composite-fiber precursors due to its low cost, ease of use, and flexibility. However, electrospinning is a time-consuming production process and faces safety due to the voltage and high current during fiber formation, especially for melt electrospinning where a high current is needed. Centrifugal spinning has emerged recently as a potential method for its high production rate of fibers and microfibers for a wide range of applications including filtration, biomedical, tissue engineering, and energy storage [9–13]. Different composite-fiber systems, such as SnO_2/C, TiO_2/C, Si/C, Sn/C and MoO_2/C, were recently prepared by centrifugal spinning and subsequent thermal treatment as potential anodes for LIBs and SIBs. [6, 8, 14, 15].

One way to improve the electrochemical performance of a composite-fiber electrode is to increase the surface area of the fibers to allow for more lithium intercalation. Exposing more surface in the active material (i.e., reactive sites) can increase the specific capacity of the electrode. One advantage of incorporating the carbon-fiber matrix into the electrode is that the carbon matrix can act as a buffer for the volume change during the lithiation/delithiation process, while taking advantage of redox active sites on the carbon-fiber surface [15]. Metal-oxide and metal-based anodes such as iron oxide and alloying compounds including silicon (Si), germanium (Ge),

tin (Sn), and others hold interesting properties such as high specific capacity and reversibility, which can be used to produce unique microstructured anode electrodes for LIBs [16, 17] [18–20]. The electrochemical performance of the composite-fiber electrode can also be improved by incorporating more active material in the composite-fiber precursor. However, increasing the concentration of the active material (e.g., metal-oxide nanoparticles) in the polymer precursor solution results in the agglomeration of NPs as well as increased surface tension and viscosity, which may affect the ability to produce centrifugally spun fibers with desirable structure and morphology. One strategy to overcome this issue is by coating the conductive fibers with the active material (using the wet coating method), which may yield significantly improved results in terms of capacity and rate performance of the composite-fiber anode [21]. This method results in composite-fiber anodes with improved electrochemical performance due to high active material loading compared to centrifugally spun composite-fiber anodes prepared from precursor solutions and subsequent heat treatment.

Binding nanoparticles to the surface of a polymer has typically been done in the context of catalysis for hydrogen and oxygen reduction reactions [22]. In this field, metal/carbon composites have been achieved by the attachment of functional carboxylic acid groups on the surface of carbonaceous materials (coating with sodium hydroxide) [23]. Metals and metal-oxide nitrogen bonded composites have also been prepared by doping with urea, or by using a nitrogen-containing polymer for the coated surface [24, 25]. Polyacrylonitrile (PAN), given its rich nitrogen and carbon content, has been used to generate unique morphologies with good potential for use in electrochemical devices [25] [21].

In the present work, PAN fibers were successfully wet-coated with cobalt (II, III) oxide Co_3O_4 thereby increasing the active material loading in the carbon-fiber matrix and thus improving the electrochemical performance of the composite-fiber electrode. The coated Co_3O_4/C composite fibers were used as anode materials for LIBs, and their electrochemical performance was systematically investigated. The synthesis method presented in this work can provide an effective avenue for the fabrication of surface coated-fiber materials for use in LIBs and SIBs.

Experimental

Materials

Polyacrylonitrile (PAN) with an average M of 150,000 g/mol, dimethylformamide (DMF) 99.5%, ethanol 9.5% and cobalt oxide nano-powder (Co_3O_4, 99%, 10–30 nm) were purchased from Sigma-Aldrich. Ethylene carbonate (EC) (99%) and dimethyl carbonate (DMC) were purchased from Alpha Aesar and Fisher Scientific, respectively. The electrolyte salt $LiPF_6$ (98%) was also purchased from Sigma-Aldrich.

Carbon fiber and anode preparation

Carbon fibers (CFs) were prepared from PAN precursor fibers by dissolving 12 wt% PAN in DMF. The solutions were stirred for 24 h using mechanical mixing to obtain homogeneous precursor solutions. Pristine PAN microfibers were obtained by centrifugal spinning at a rotational speed ranging from 6500 to 8000 rpm and relative humidity below 40% (Fig. 1). The fibers were then collected on a rectangular aluminum substrate and subsequently dried under vacuum at 60 °C. After drying, the fibrous mat was stabilized in air at 280 °C in an OTF-1200X tube furnace (MTI Corp. California, USA) for 4 h (heated at a rate of 3 °C/min), which was followed by carbonization under argon atmosphere at 600 °C for 6 h.

Preparation of coated carbon fibers

The Co_3O_4-coated carbon fibers (CCFs) were prepared by dispersing low concentrations of Co_3O_4 nanopowder into ethanol and stirring for 5 h. Subsequent to stirring, the mixture was sonicated for 1 h. The fibrous PAN mats were weighed and coated with 30, 50, or 70 wt% of Co_3O_4 nanoparticles (CCF30, CCF50 and CCF70, respectively). The fibrous mats were placed flat on a surface where a proper amount of solution was poured and sonicated for 1 h. The samples were then dried at room temperature for 24 h prior to heat treatment. In this process, the coated fibers were placed in an OTF-1200X tube furnace, stabilized under air at 280 °C for 4 h (heated at a rate of 3 °C/min), and carbonized under argon atmosphere at 600 °C for 6 h.

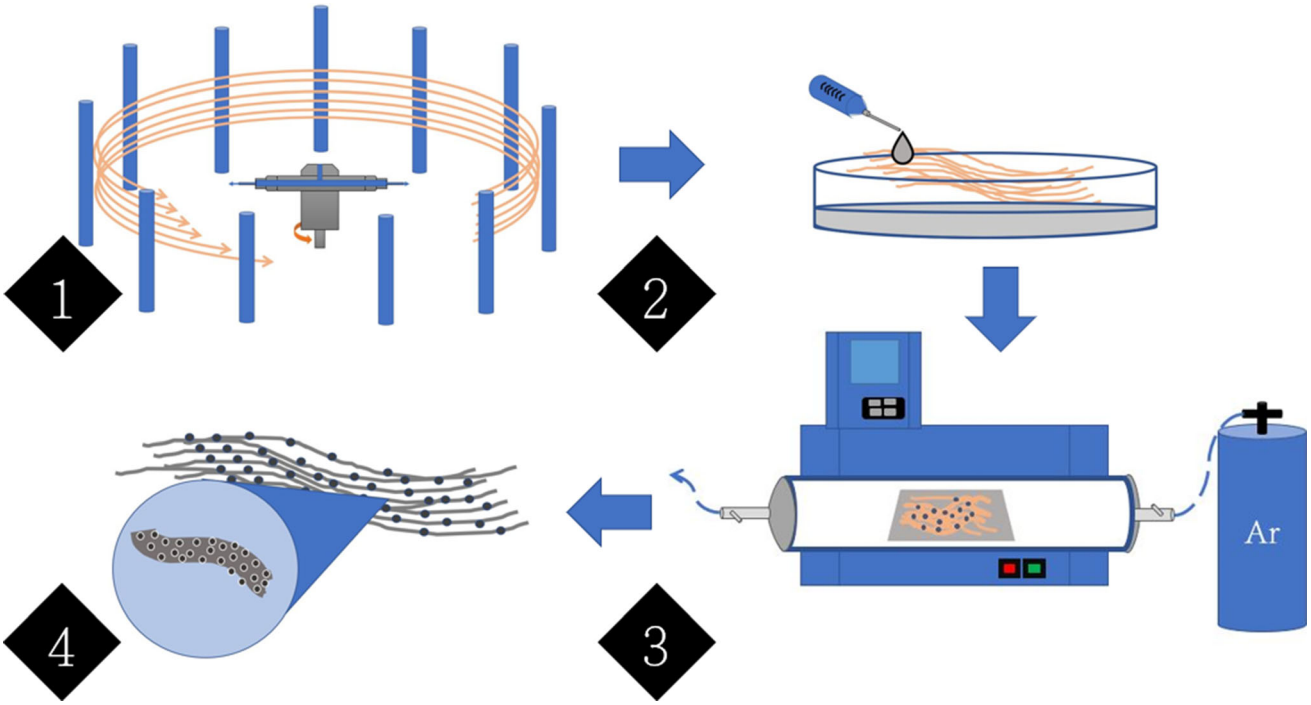

Figure 1 Schematic showing processing of composite-fiber electrodes.

Characterization

The composite fibers were characterized using X-ray diffraction (XRD) before and after carbonization. The diffraction patterns were collected in 2θ from 10° to 80°, with a step of 0.05° and a 5 s counting time, using a Bruker D2 X-ray diffractometer. Scanning electron microscopy (SEM) imaging and energy-dispersive X-ray spectroscopy (EDS) were collected using a Sigma VP Carl Zeiss scanning electron microscope with an attached EDAX detector (EDAX, Mahwah, NJ, USA). Transmission electron microscopy (TEM) images and selected area electron diffraction (SAED) images were recorded using a FEI G2 F30 microscope operated at 300 kV. High-angle annular dark field (HAADF) scanning TEM (STEM) and EDS maps were collected with a FEI G2 Titan 60–300 probe corrected microscope equipped with a Super-X EDS system. The Titan was operated at 200 kV with a convergence semi-angle of 24 mrad and HAADF inner collection semi-angle of 58.5 mrad. X-ray photoelectron spectroscopy (XPS) data were collected using a Thermo Scientific *K*-Alpha X-ray Photoelectron Spectrometer to characterize surface composition of the CFFs. Thermogravimetric analysis (TGA) was performed using a Netzsch Tarsus TG 209F3 to determine the amount of cobalt oxide present in the CFF anodes.

Electrochemical experiments and half-cell preparation

Before use in the Li-ion half cells, the CCF anodes were dried under vacuum at 60 °C overnight to prevent moisture in the sample. The anodes were weighed and placed into a MBRAUN (LABstar pro) glove box filled with ultra-high purity argon with H_2O and O_2 concentrations of < 0.5 ppm. They were assembled using CR2032 coin cells by employing a lithium chip as the counter electrode. Cyclic voltammetry (CV) experiments were performed using Biologic (MCS810) at a scan rate of 0.2 mVs^{-1} over the range from 0.01 to 3.0 V (vs. Li/Li^+). Galvanostatic charge and discharge experiments were performed using a LANHE battery testing system (CT2001A) over the same voltage range at room temperature using charge/discharge rates of 100 and 200 mA g^{-1}. Li-ion half cells were also tested using an Arbin

automatic battery cycler to evaluate the rate performance at current densities of 50, 100, 200, 400, and 500 mA g^{-1} between cutoff potentials of 0.01 and 3 V. The electrochemical impedance spectroscopy experiments were performed over the frequency range from 1 kHz to 0.005 Hz using a Metrohm Autolab (PGSTAT 128 N, Metrohm).

Results

Surface morphology and characterization

Figure 2 shows SEM images of CFs and CCFs after carbonization of the precursor fibers. The fiber diameter distribution (histograms) of CFs and CCFs are also shown in Fig. 2. The average fiber diameter

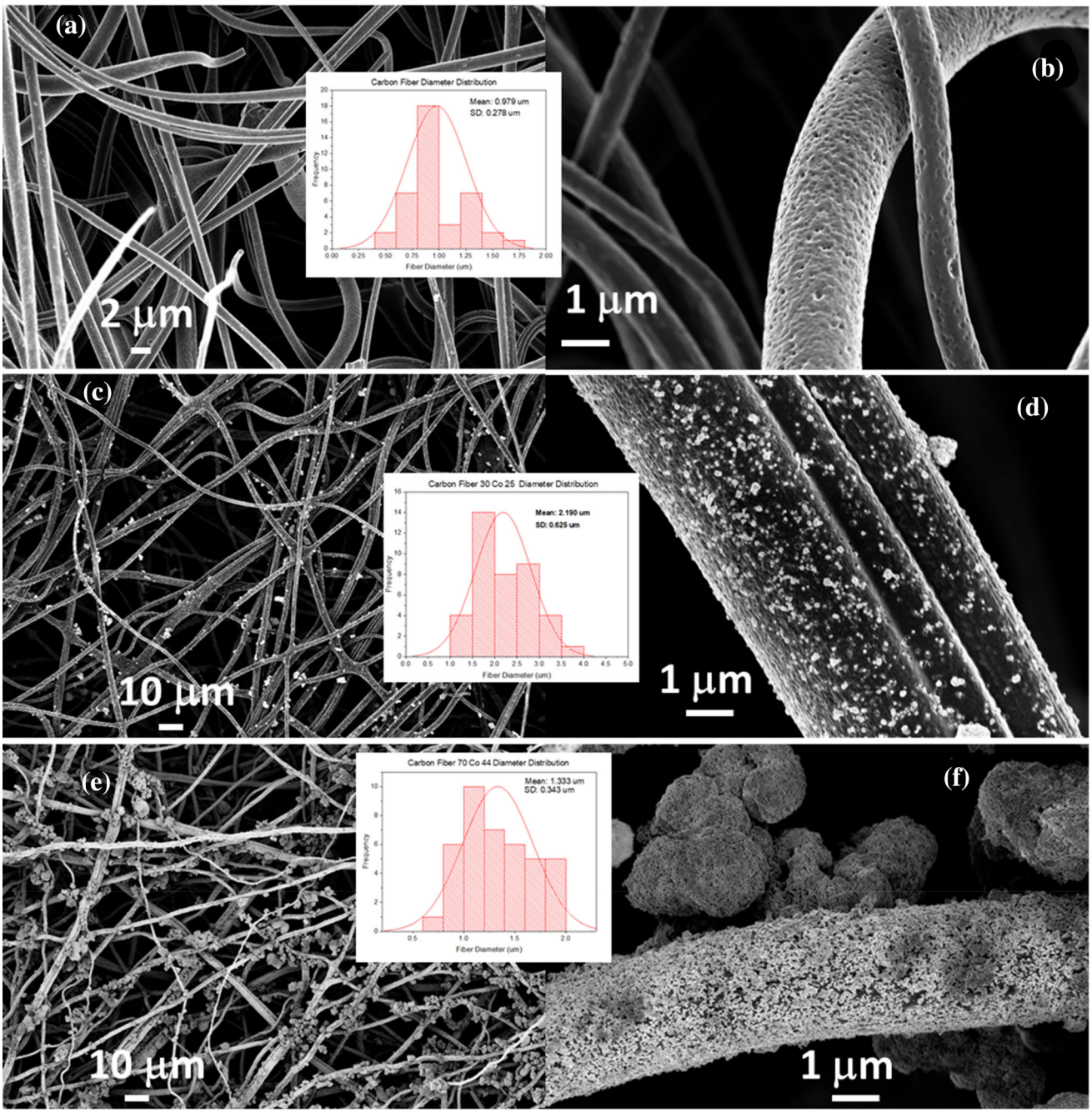

Figure 2 SEM and size distribution of CF anode (**a** and **b**), CCF30 (**c** and **d**), the CCF70 **e**), and **f**). Insets show the fiber diameter distribution (histograms).

of the CFs was approximately 1 μm, while the diameter of the CCFs was between 1.5 and 2 μm. The presence of agglomerated nanoparticles on the surface of the PAN fibers may have prevented some loss of mass as can be observed with the increase in diameter compared to the uncoated samples (CF). Alternatively, the Co_3O_4 NPs on the surface may be partially embedded into the CFs, which would cause an increase in the fiber diameter compared to the pristine CFs. The SEM images in Fig. 2 show a good dispersion of Co_3O_4 nanoparticles on the carbon fibers. To avoid moisture in the atmosphere from being absorbed by the metal-oxide nanoparticles, the Co_3O_4 NPs were stored in a large desiccator prior to mixing with ethanol. The low concentration of nanoparticles enabled uniform coating on the surface of the PAN fibers, although some agglomeration of the Co_3O_4 NPs on the fiber surface was apparent at higher Co_3O_4 concentrations nearing 60 wt%. The surface defects on the fibers, which can be observed in Fig. 2a, may have helped the cobalt nanoparticles adhere to the surface of PAN fibers.

The XRD and SAED patterns of cobalt oxide nanoparticles and carbon-fiber electrode (Fig. 3) confirm the presence of Co_3O_4 NPs on the carbon fibers. Both patterns (SAED and XRD) showed the Co_3O_4 nanoparticles present in cubic form with space group of Fd-3 m and lattice parameters of $a = b = c = 8.087$ Å and $\alpha = \beta = \gamma = 90°$, which is consistent with results reported on the structure of Co_3O_4 nanocrystals [26, 27]. Figure 3 shows the powder XRD pattern (C) for the CCFs, the SAED pattern (C), and the area used for the SAED (D). The diffraction pattern for the Co_3O_4 nanoparticles (Fig. 3a) shows the 111 (22.11° 2θ), 200 (25.59° 2θ), 220 (35.40° 2θ), 311 (43.09° 2θ), 222 (45.11° 2θ), 400 (52.58° 2θ), 331 (57.72° 2θ) 420 (59.36° 2θ), 422 (65.70° 2θ), 511 (70.25° 2θ), 333 9 (70.25° 2θ) and 440 (77.56° 2θ) diffraction planes for the Co_3O_4 phase. The XRD pattern after heat treatment (Fig. 3b) shows the 111 (22.11° 2θ), 200 (25.59° 2θ), 220 (35.40° 2θ), 311 (43.09° 2θ), 222 (45.11° 2θ), 400 (52.58° 2θ), 331 (57.72° 2θ) 420 (59.36° 2θ), 422 (65.70° 2θ), 511 (70.25° 2θ), 333 9 (70.25° 2θ) and 440 (77.56° 2θ) diffraction planes for the Co_3O_4 phase. Figure 3b also shows the 111 (42.74° 2θ), 200 (49.76° 2θ), and 220 (73.03° 2θ) diffraction planes for the CoO, and the 111 (51.82° 2θ) and 200 (60.61° 2θ) planes for the Co metal. Both the SAED and powder XRD patterns show a change in the structure of the Co_3O_4 NPs after heat treatment and the appearance of new Co containing phases. The results in Fig. 3 also confirm the presence of three different phases in the Co_3O_4 coated carbon fibers samples: Co_3O_4, Co metal, and CoO [28–30]. The reduction reaction of cobalt oxides to Co or CoO in the presence of carbon at high temperatures has previously been reported [31–33].

Figure 3e, f shows a high-resolution HRTEM image with the measured *d*-spacing in the Co_3O_4 nanocrystals. The lattice spacing observed in the figure was consistent with the inter-planar spacing for Co_3O_4 crystals. The distances between adjacent lattice planes were measured and found to have spacings of 2.42, 2.86, and 4.66 Å which are consistent with the (311), (220) and (111) *d*-spacings observed in the XRD results and also in agreement with results reported on the same material [34–36].

Figure 4a, b shows HRTEM images of the Co_3O_4 nanoparticles embedded in carbon fibers and possibly protruding through the surface (Fig. 4a). The nanoparticles were observed to exist in different geometries, which consisted of spherical, rod shaped, and irregular shapes. The amorphous grey structure in the HRTEM images represents carbon fibers.

Figure 4b shows the presence of both the carbon fibers and Co_3O_4 nanoparticles close to the carbon-fiber matrix, while some nanoparticles are embedded in the fibers. In addition, some carbon fibers show graphitic character, which is represented by the alignment of the atoms in the structure. Figure 4c is a lower-magnification TEM image of the sample, which shows that the Co_3O_4 nanoparticles are clustered on the surface of the carbon fibers, while some of the particles are embedded in or protruding from the fibers. The EDS mappings and bright-field images of the Co_3O_4/C composite fibers are shown in Fig. 4c–h. It can be observed in Fig. 4d–h that the CCFs sample consists of carbon, nitrogen, oxygen, and cobalt. The EDS mappings of the carbon and nitrogen correlate closely with one another, which is consistent with using PAN as the carbon source. The light carbon present in the background of the EDS mapping (Fig. 4d) is due to the carbon-coated grid used for the TEM. In addition, the sample was carbon-coated for the TEM data collection and analysis. Furthermore, there is a high correlation between the presence of Co and O in the EDS mappings, confirming a cobalt oxide structure. However, there is also a correlation among the positions of the O, N, and Co in the elemental maps. The elevated N concentrations from the carbonized PAN fibers correlate with the positions of

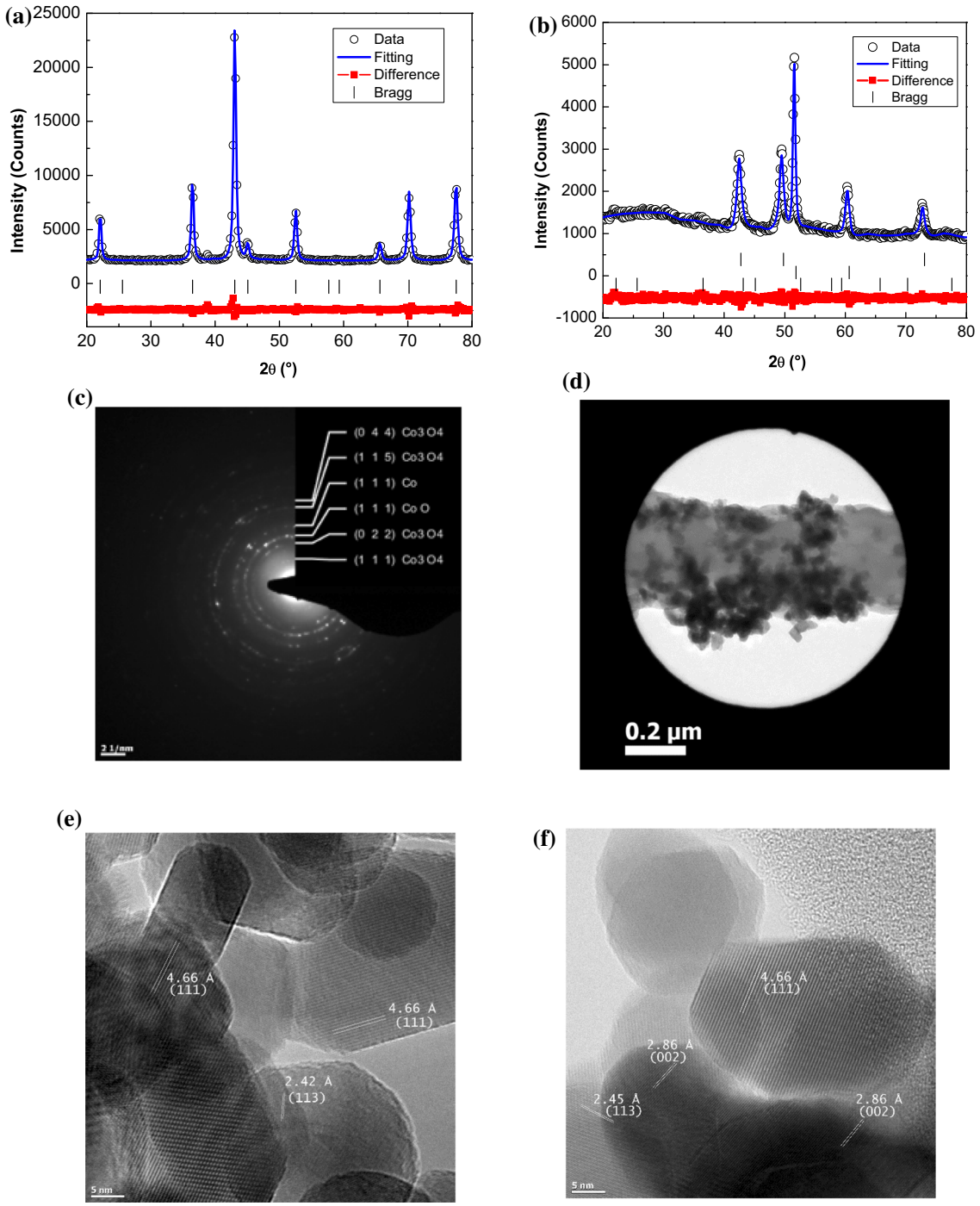

Figure 3 **a** Powder X-ray diffraction pattern of the Co_3O_4 nanoparticles. **b** Powder X-ray diffraction pattern of the Co_3O_4 nanoparticles as synthesized in carbon fibers. **c** SAED pattern of Co_3O_4 nanoparticles as synthesized in carbon fibers, **d** TEM image of Co_3O_4 nanoparticles as synthesized in carbon fibers used to collect the SAED data. **e** HRTEM of Co_3O_4 nanoparticles as synthesized. **f** HRTEM of Co_3O_4 nanoparticles.

high concentrations for both Co and O in the sample. This might indicate that the existence of residual N in the PAN fibers after carbonization was the point of attachment or bonding for the Co_3O_4 nanoparticles. In addition, the presence of N in proximity to the CoO nanoparticles may help explain the observed reduction of Co_3O_4 to a combination of Co metal and CoO. The lone pair of elections on N may have been

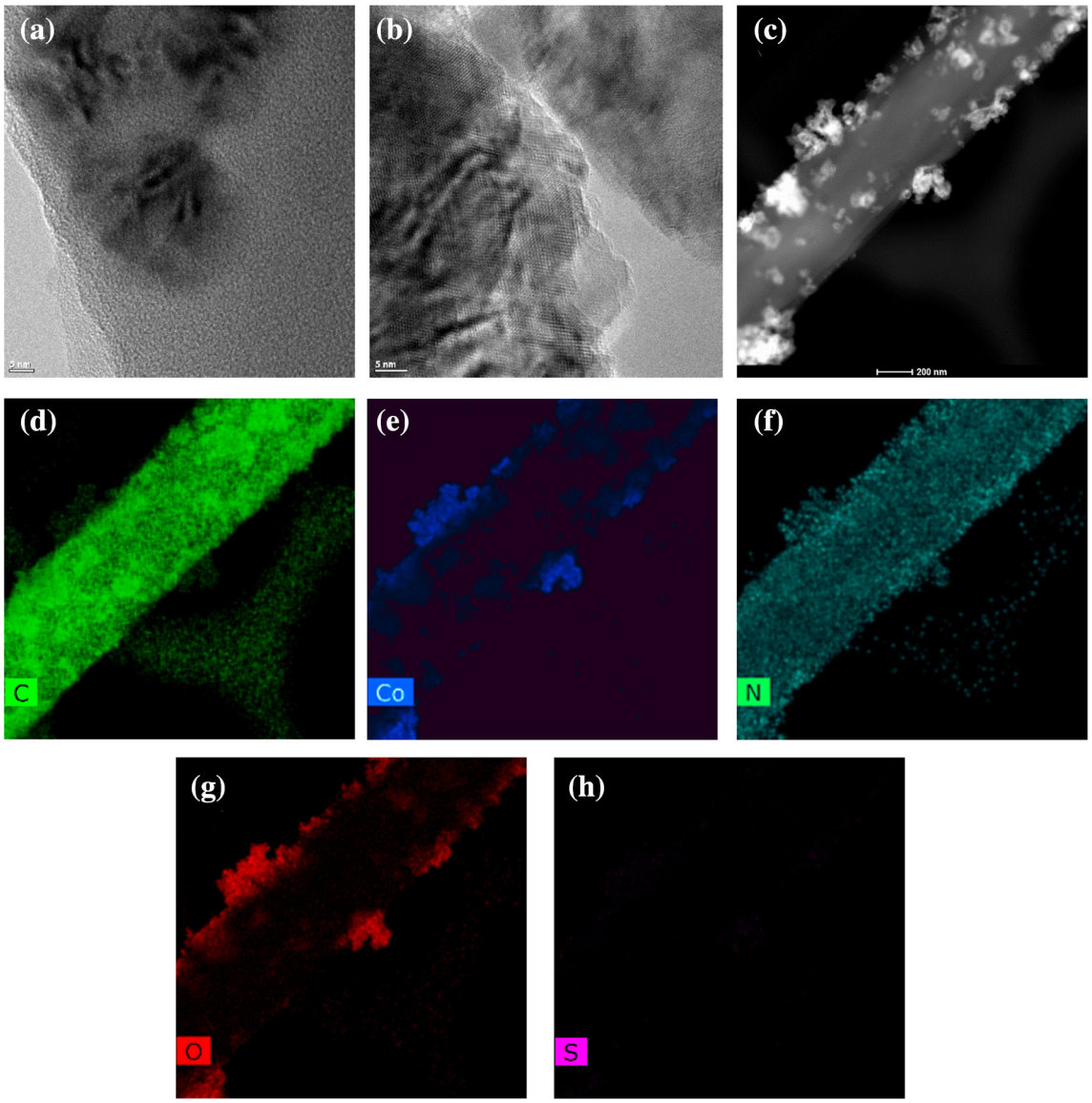

Figure 4 HRTEM image of Co_3O_4 nanoparticles embedded in carbon fibers (**a**), HRTEM of the as-synthesized Co_3O_4 nanoparticles embedded in carbon fibers (**b**), and TEM image of Co_3O_4 nanoparticles, embedded and deposited on the surface of the carbon fibers (**c**), EDS mapping of C (**d**), Co (**e**), N (**f**), O (**g**), and S (**h**) of the Co_3O_4/C composite fibers.

used to reduce the Co_3O_4 during the carbonization process and then contribute to a stronger bond between the Co_3O_4/Co/CoO and the fibers.

XPS analysis

To further understand the bonding of the nanoparticles to the carbon fibers, XPS analysis was performed on the CFF anodes. Figure 5a shows the broad survey spectrum for the collected XPS data, in which the presence of C, O, N, and Co after the carbonization is detected. Figure 5b shows the Co 2P of the samples after carbonization of the Co/PAN composite fibers. This spectrum can be broken down into two regions for the Co $2P_{3/2}$ and the C o2$P_{1/2}$ at 779 and 795 eV, respectively. The Co $2P_{3/2}$ peak was deconvolved into four different peaks located at 778.5, 799.8, 781.7, and 786.2 eV. The peak located at 778.5 eV is present due to the reduction of the cobalt to Co metal nanoparticles [37]. The peak at 779.8 eV is associated with the presence of Co^{3+}, while the peak located at 781.2 eV represents the Co^{2+} $2P_{3/2}$. The final peak located at 786.2 eV is the Co $2P_{3/2}$ satellite peak observed in the Co–O bonding environment.

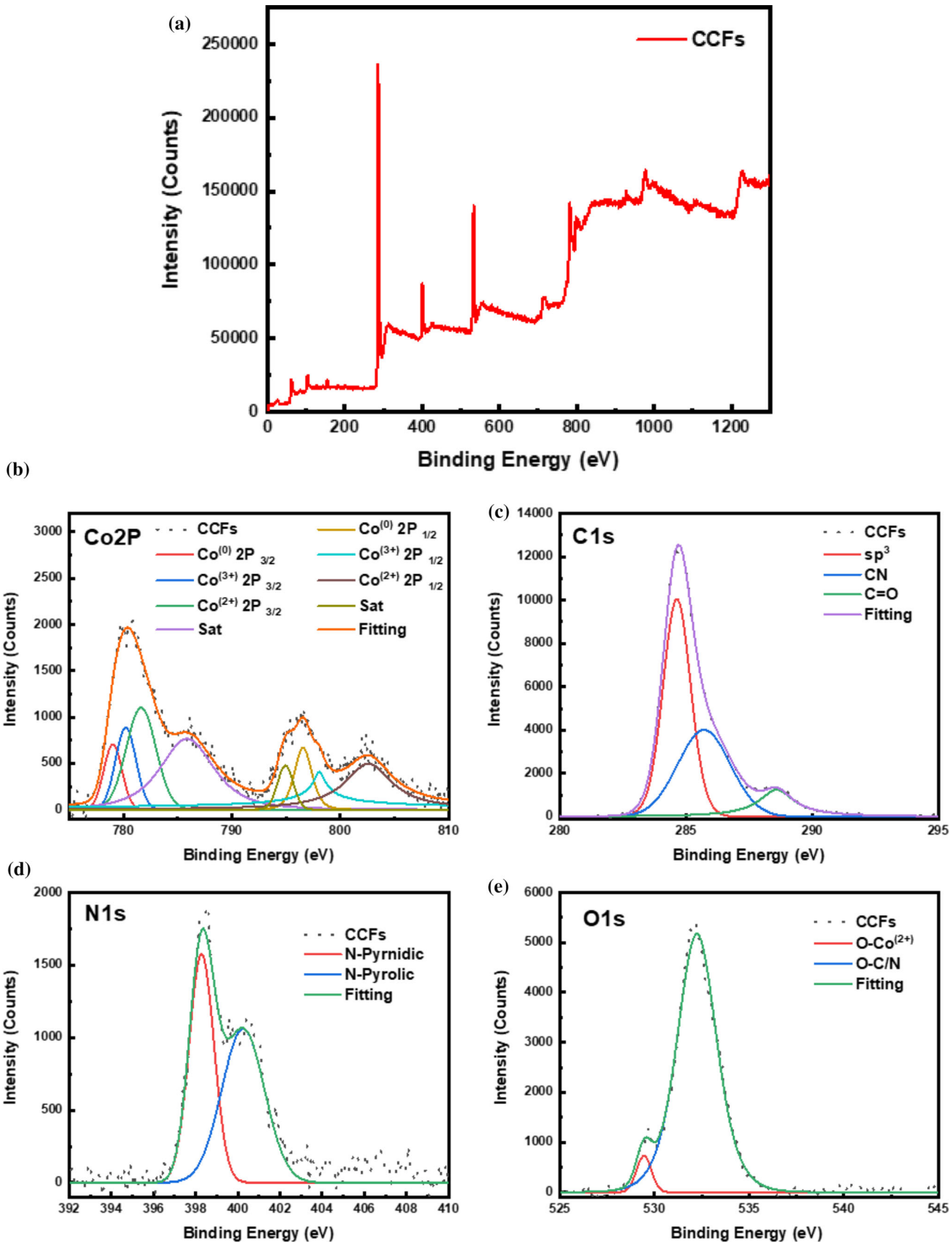
(a)
CCFs
Intensity (Counts)
Binding Energy (eV)
(b)
Co2P
CCFs
Co(0) 2P 3/2
Co(3+) 2P 3/2
Co(2+) 2P 3/2
Sat
Co(0) 2P 1/2
Co(3+) 2P 1/2
Co(2+) 2P 1/2
Sat
Fitting
Intensity (Counts)
Binding Energy (eV)
(c)
C1s
CCFs
sp3
CN
C=O
Fitting
Intensity (Counts)
Binding Energy (eV)
(d)
N1s
CCFs
N-Pyrnidic
N-Pyrolic
Fitting
Intensity (Counts)
Binding Energy (eV)
(e)
O1s
CCFs
O-Co(2+)
O-C/N
Fitting
Intensity (Counts)
Binding Energy (eV)

◀**Figure 5** **a** XPS survey of Co_3O_4 nanoparticles in the carbonized PAN fibers (CFFs). **b** Co_2P **c** C 1S **d** N1S, and **e** O1S scans of Co_3O_4 /C composite fibers (CFFs).

Similarly, the Co $2P_{2/1}$ peak can be deconvolved into four peaks located at 794.5, 796.2, 797.8, and 802.8 eV. The peaks represent the Co (0), Co^{3+}, Co^{2+}, and the Co–O satellite features, respectively. The C 1S spectrum for the PAN fibers with Co_3O_4/C composite fibers is shown in Fig. 5c, which was deconvolved into three individual peaks located at 284.7, 285.8 and 288.6 eV. These peaks are representative of the C–C/C=C, C=N, and C=O binding environment, respectively [38]. The N 1S spectrum of the Co_3O_4 /C composite fibers is shown in Fig. 5d. The spectrum was deconvolved into two nitrogen environments, the pyrrolic and pyridinic, located at 398.3 and 399.3 eV, respectively. These two nitrogen environments are commonly observed in PAN fibers after stabilization and carbonization. The O 1S spectrum for Co_3O_4/C composite fibers is shown in Fig. 5e. The spectrum was deconvolved into two peaks located at 529.5 and 532.2 eV, which are representative of the Co–O and C/N–O environments within the sample. In summary, the XPS data corroborate the XRD in confirming the presence of CoO, Co_3O_4, and Co metal. Also, the XPS data show that the nitrogen- and oxygen-containing ligands in the CFs are the point of attachment for the Co_3O_4 nanoparticles, as also inferred from the EDS data.

TGA analysis

Figure 6 shows TGA thermograms of carbon fibers (CF), and composite fibers CCF30, CCF50, and CCF70. The experiments were performed under air atmosphere over a temperature range between 25 and 900 °C at a heating rate of 10 °C min^{-1}. A 5% weight loss was observed for all CCF samples at a temperature below 200 °C, while a 10% weight loss was observed for CFs. This initial loss is attributable to the removal of water from the samples. The cobalt oxide content in the fibers correlates well with that used in the precursor solutions to prepare the Co_3O_4-coated PAN fibers. It can be observed in Fig. 6 that the residual mass in the CF, CCF30, CCF50 and CCF70 samples is 5, 27, 50 and 60 wt%, respectively.

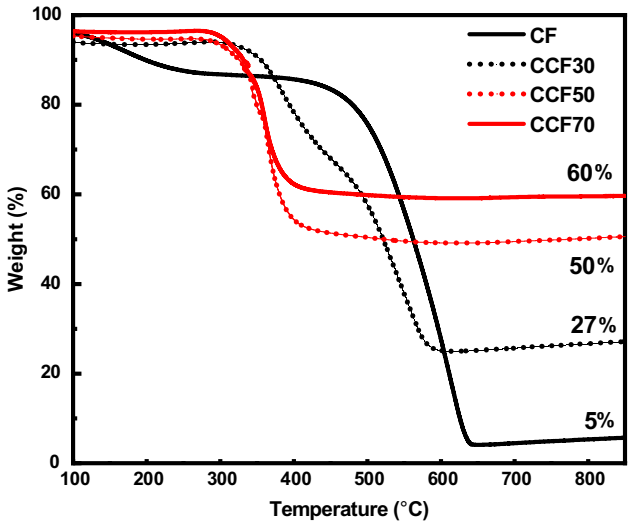

Figure 6 TGA curves of CF, CCF30, CCF50, and CCF70 samples, obtained at 10 °C min^{-1}.

Electrochemical performance

Figure 7 shows cyclic voltammetry (CV) results of CF (A) and CFF70 (B) composite electrodes during the first four scans at a rate of 0.2 mV s^{-1}. It is observed in Fig. 7a that the carbon-fiber electrode shows obvious cathodic peaks close to 0.75 V and anodic peaks at ca. 0.35 V, corresponding to the Li^+ intercalation/deintercalation reactions. In the first cathodic scan (lithiation) of the CFF70 electrode (Fig. 7b), a peak is observed at ca. 0.55 V which is assigned to the reduction of cobalt oxide species (CoO, Co_3O_4) into Co [39–42]. This reduction peak was shifted to lower voltage in the subsequent cathodic scans indicating the occurrence of some irreversible reactions, such as those of cobalt oxide with lithium ions to form Li_2O [43–45]. The intensity of this oxidation peak decreases during the subsequent anodic scans.

The charge–discharge curves for carbon-fiber anodes with different concentrations of cobalt oxide (0, 30, 50, 70%) are shown in Fig. 8. During the first discharge cycle (lithiation), the anode potential drops to a voltage of less than 2 V (1.25 V for that charged at 200 mA g^{-1}) followed by long voltage plateaus observed in the range of 0.5–0.75 V. These voltage plateaus are characteristic of cobalt (Co_3O_4 and CoO) [36, 37]. The rapid initial loss in capacity from the first to 10th cycles can be attributed to the formation of a large SEI layer on the surface the composite-fiber anodes. It should be noted that the charge and discharge curves follow similar profiles after 10 cycles.

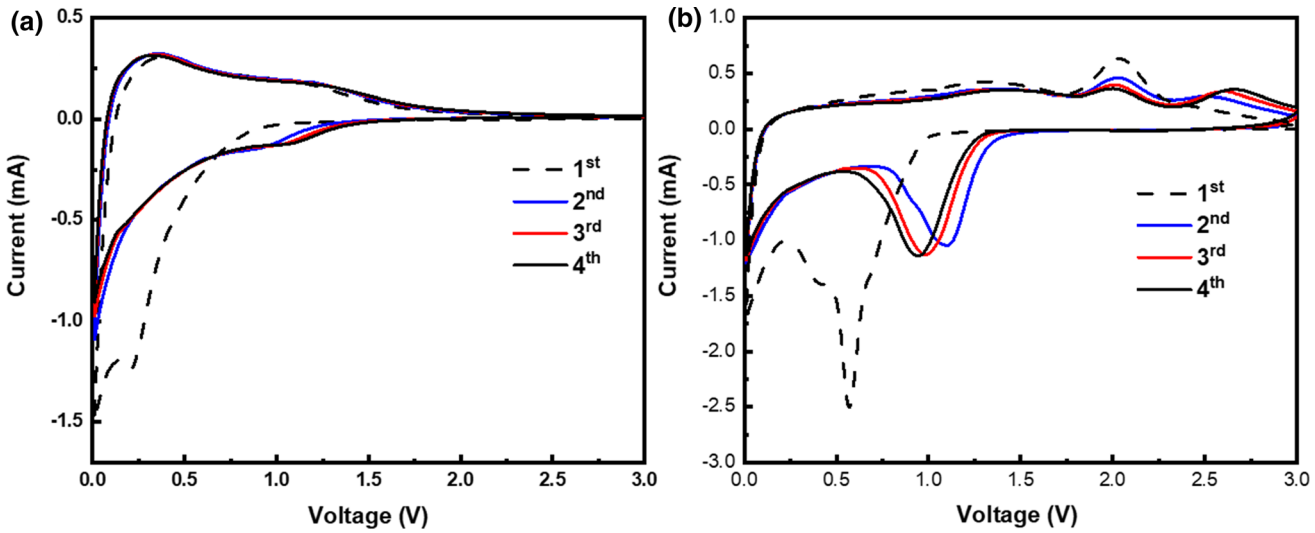

Figure 7 Cyclic voltammetry of CF(A) and CFF50 (B) in a half-cell configuration and cycled between 0 and 3.0 V at a scan rate of 0.2 mV s^{-1}.

The CCF composite anodes exhibited specific capacities of 625 mAh g^{-1} (CCF50) at 100 mA g^{-1}, and 300 mAh g^{-1} (CCF30), 420 mAh g^{-1} (CCF70) when cycled at 200 mA g^{-1} (Fig. 8c, d). The results indicate good stability of all CCF anodes with Co_3O_4 content up to 70 wt%. Additionally, there was a loss in specific capacity at increasing cycle number, which can be due to the high-volume change upon cycling as well as to the side reactions of lithium with oxygen to form LiO_2. Despite some losses in capacity and Coulombic efficiency at the first cycle, the CCF electrodes show almost double the specific capacity (Fig. 7b) of that for the pristine carbon-fiber anode (Fig. 7a). At a current rate of 200 mA g^{-1} and lower Co_3O_4 concentrations (CCF30), the composite-fiber electrodes still deliver a higher capacity when compared to carbon fibers.

Figure 9a shows the cycle performance after 100 cycles of CFs and CCF50 at 100 mA g^{-1}, CCF30 and CCF70 at 200 mAg^{-1}. The breakdown and solidification of the electrolyte at the anode/electrolyte interface during the first discharge cycle is reflected in the loss of charge capacity after the first cycle (Li-deintercalation + conversion). This effect is amplified by the large surface area of the micro-fibrous mat, which contributes to the SEI formation at the first discharge cycle, resulting in a high irreversible capacity. However, the specific reversible capacity of carbon fibers remained stable after 100 charge/discharge cycles, suggesting that a good cyclability was observed for the CF and CCF anodes. After 100 cycles, the CCF30 delivered a slightly higher specific capacity than that of CF anodes (300 mAh g^{-1}), while CCF70 showed a specific capacity of 420 mAh g^{-1} after 100 cycles.

Figure 9b shows the Coulombic efficiency of CFs and CCF50 at 100 mA g^{-1}, CCF30 and CCF70 at 200 mAg^{-1}. The results in Fig. 9b show clearly that the initial Coulombic efficiency (ICE) is low at the first cycle and this is due to the formation of a thick SEI layer on the fiber-anode surface. This resulted in a high consumption of Li ions by the CFs AND Co3O4/C composite fibers and hence a high irreversible capacity, as observed in Fig. 8a–d. This phenomenon is known as the irreversible consumption of lithium for the SEI formation; see [46]. However, the Coulombic efficiency in Fig. 9b still achieves about 97–100% after the second cycle, indicating good performance and high reversible capacity of the CF and Co_3O_4/C composite-fiber anodes after the first cycle.

The rate performance results (charge capacity vs. cycle number) of CF and CCF anodes cycled at 50, 100, 200, 400, and 500 mA g^{-1} are shown in Fig. 9c. The performance of CCFs showed good cycling stability and higher specific capacity when compared to the carbon fibers (CFs). At low current rates, the effect of the Co_3O_4 concentrations on the rate performance of the CCF composite electrodes is observed in the large gap in specific capacity where the higher concentration of active material resulted in a higher capacity of the composite anode. However,

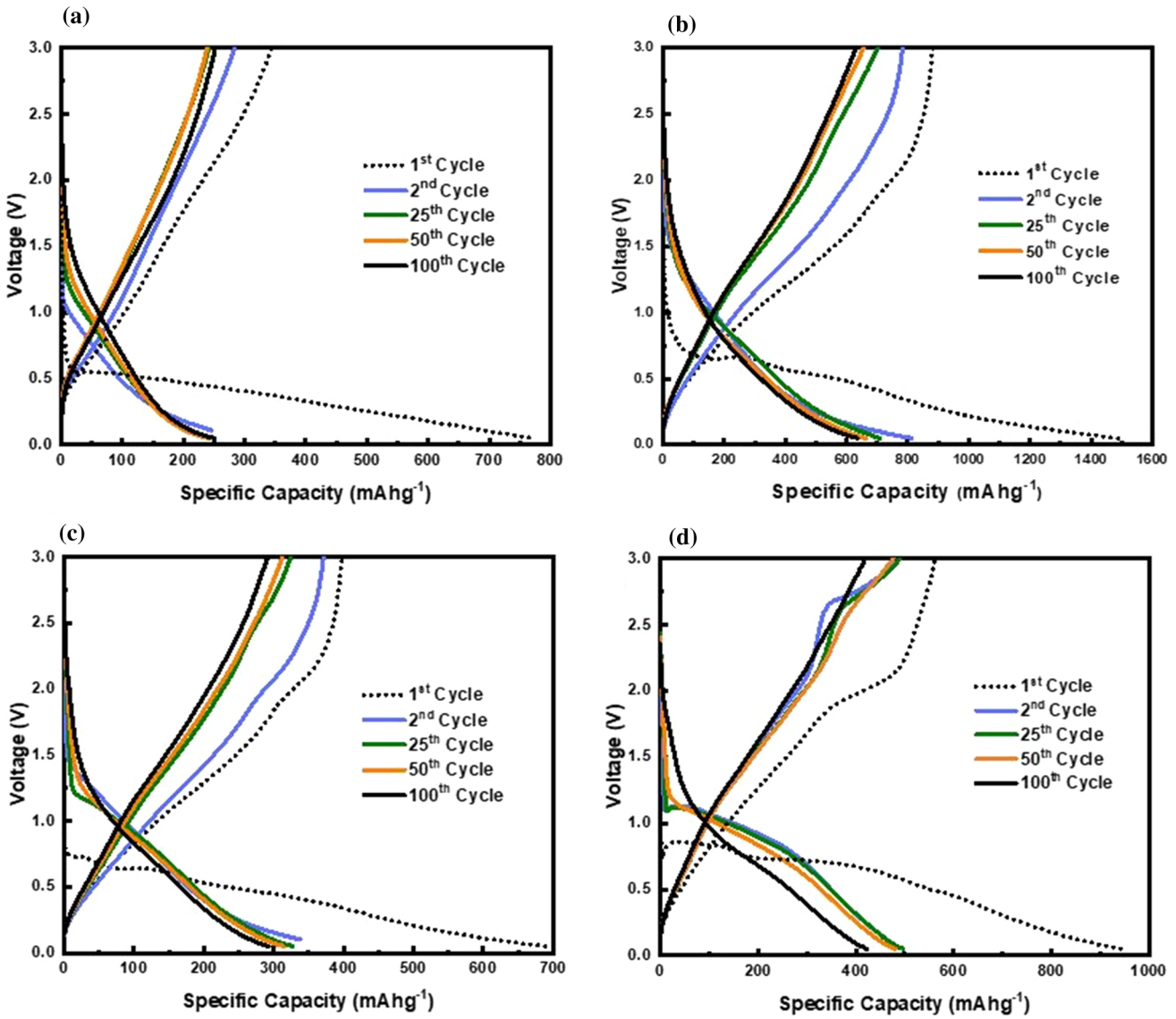

Figure 8 Galvanostatic charge/discharge profiles of **a** CF, **b** CCF50 at 100 mA g^{-1}, and **c** CCF30(C), **d** CCF70(D) at 200 mAg^{-1} at a cutoff voltage between 0.1 and 3 V.

at higher charge/discharge rates, increasing the concentration of active material did not yield a significant improvement in specific charge capacity of CFF anodes. When cycled at the original charge rate of 50 mA g^{-1}, the CF and CFF anodes delivered similar capacities to that at the first rate of 50 mA g^{-1}, indicating good capacity retention and stability of the anodes after charging/discharging at higher rates.

The results shown in Fig. 9 indicate that the Co_3O_4/C composite-fiber anodes exhibited higher capacity and better rate performance than that for CFs anode. It is worth noting that a cobalt-based anode material is expensive compared with other anode materials used in LIBs. However, the surface-coating method discussed in this work may have a high impact on the processing of binder-free anodes by centrifugal spinning at a high production rate compared to electrospinning. Using 30–40% active material (e.g., cobalt oxide) in a polymer precursor solution or coating the PAN fibers with 30–40% Co_3O_4 nanoparticles can result in composite-fiber anodes with a capacity twice that of carbon-fiber or graphite anodes. Another approach could be to start with a cobalt oxide precursor rather than already synthesized Co_3O_4 nanoparticles. This would reduce the total cost of anode. Also, the large production rate

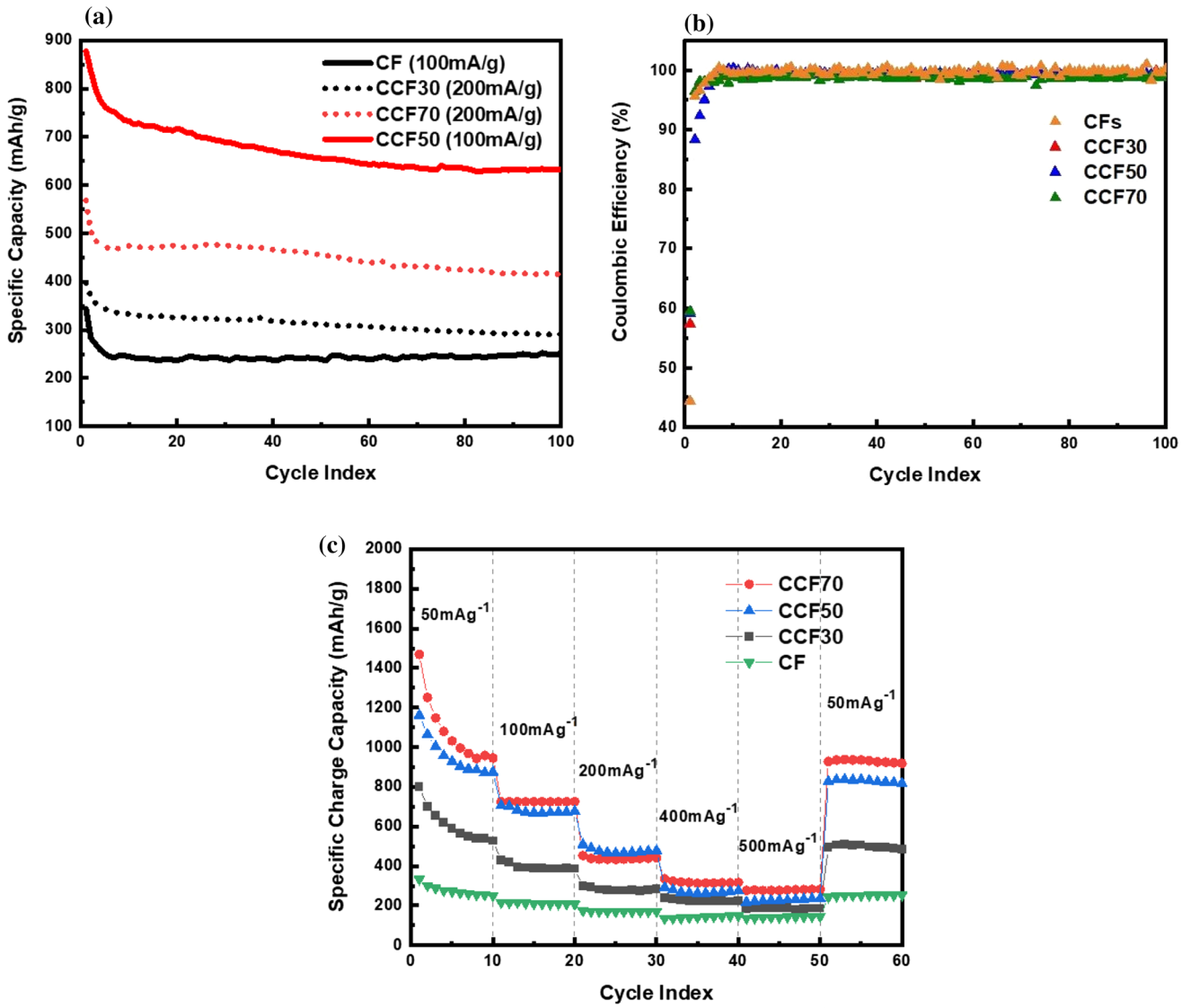

Figure 9 **a** Cycle performance of CF and CCF50 at 100 mA g^{-1}, CCF30 and CCF70 at 200 mAg^{-1}. **b** Coulombic efficiency of CF and CCF50 at 100 mA g^{-1}, CCF30 and CCF70 at 200 mAg^{-1}. **c** Rate performance of CF, CCF30, and CCF70 in Li-ion half cells.

of coated Co_3O_4/C composite anodes would compensate for the high cost of the cobalt material. Besides, cobalt-based materials have some advantages over graphite anodes, such as high theoretical capacity, rich redox reactions, and adequate cyclability; see [47]. Again, the focus in this paper is on the synthesis (coating) method; cobalt oxide was chosen as the active material just to prove the effectiveness of this surface-coating method in improving the cycle performance of centrifugally spun composite-fiber anodes. More importantly, Co metal that results from the conversion reaction of Co_3O_4 with Li at the first discharge cycle can also act as a catalyst for the decomposition and formation of Li_2O, which can contribute to the reversible transition of Li ions (from anode to cathode) during the charge (delithiation) cycle; see [48].

Electrochemical impedance spectroscopy (EIS) experiments (Nyquist plot) were performed on the Co_3O_4/C composite-fiber electrodes before and after cycling at 100 mA g^{-1} (Fig. 10). The semicircle observed in the medium to high frequency range is associated with different electrochemical processes within the cell. These processes include the SEI formation, contact resistance between materials, and reduction of cobalt oxide on the surface of the carbon fibers [49] [50]. Figure 10b shows tabulated results for the modeling of the EIS spectra. In the equivalent

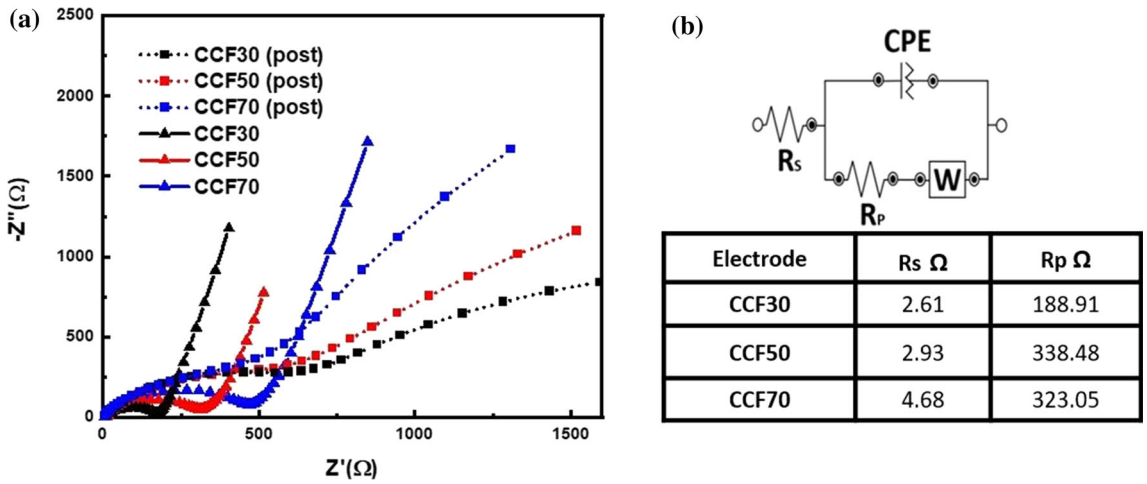

Electrode	Rs Ω	Rp Ω
CCF30	2.61	188.91
CCF50	2.93	338.48
CCF70	4.68	323.05

Figure 10 **a** Electrochemical impedance results (Nyquist plots) of fresh and aged Li-ion half cells containing CCF electrodes with different Co_3O_4 constrictions. **b** Impedance table showing R_s, R_P, and equivalent circuit model of the CCF anodes.

circuit model (Fig. 10b), R_s is the electrolyte solution resistance, R_p is the charge transfer resistance, W is the Warburg impedance of Li-ion diffusion into the active material at low frequency, and CPE is the constant phase-angle element equivalent to the double layer capacitance. With the increase in cobalt oxide content, the diameter of the semicircle increased because of the increase in the contact resistance at the electrode/electrolyte surface. When compared to freshly assembled cells, the aged cells (post cycled) showed larger and incomplete semicircles followed by a tail with a lower slope than that for the fresh cells. This indicates that a slower diffusion took place in the low frequency range after 100 cycles. Higher concentrations of active material in the carbon fibers led to faster diffusion in the low frequency range (after 100 cycles), which is attributable to the greater amount of active material trapped in the carbon fibers after lithiation. Similar EIS results have been reported previously for cobalt oxide electrodes [51].

Discussion

It is well accepted in the battery research community that new direction for battery materials is to design high capacity anodes with stable performance. Also, the design of a good cathode is very important to make sure that the high capacity anode is fully lithiated during repeated discharge cycles in a full cell configuration. However, the focus of the present manuscript is on the synthesis and design of centrifugally spun and free-standing composite-fiber anodes. The novel synthesis (coating) method used in this work focuses on the large scale production of binder-free Co_3O_4/C composite-fiber anodes with a stable capacity, and also to address the difficulties encountered during the centrifugal spinning of composite precursor solutions containing active material (nanoparticles, nanoroads, nanotubes). It is well known that free-standing electrodes (binder-free electrodes) will result in improved electrochemical performance of the battery due to the elimination of electrochemically inactive material in the slurry electrode (specifically from the current collector); see [52].

Moreover, the CF and Co_3O_4/C composite-fiber anodes showed a good Coulombic efficiency (CE) between 97 and 100% after the first cycle (Fig. 9b). However, these anodes showed a low ICE at the first cycle which was caused by the SEI formation and high surface area of the fibers. In general, the Coulombic efficiency of the anode at the first cycle is low due to the formation of the SEI layer in the first cycle and the decomposition of the electrolyte at the anode surface. For the case of electrospun or centrifugally spun composite nanofibers, the SEI layer becomes thicker than that for conventional slurry-based electrodes due to the high surface area of the nanofibers, nanotubes, or nanorods and can result in a low initial Coulombic efficiency (ICE) at the first cycle. A thick SEI layer can consume a large amount of Li ions and electrolyte at the first discharge (Li-

insertion) cycle, thus resulting in a high irreversible capacity and low ICE; see [53–55].

As mentioned above, to date, the majority of anodes show a low ICE at the first cycle, which is a major issue that needs to be addressed when using commercial or laboratory-scale Li-ion full cells. In the case of Li-ion half cells, the low ICE at the first cycle does not really affect the electrochemical performance of the anode since there is unlimited source of Li + provided by the Li-metal counter electrode to the working electrode (i.e., CF and Co_3O_4/C composite fibers used in this work). However, in commercial Li-ion cells this issue is very vital and needs to be addressed since there is a limited source of Li ions provided by the cathode to the anode during repeated charge/discharge cycles. The SEI formation and electrolyte decomposition issues are being investigated by many researchers. For example, the incorporation of additives in the organic liquid electrolytes can improve the loss in the first capacity at the first cycle and improve the initial Coulombic efficiency; see [56–58].

Another approach that has been used to increase the ICE is first to discharge the anode and charge the cathode and then couple them in a full cell configuration; see [59, 60] Furthermore, pre-lithiation of the anode is a another method that has been widely used to overcome the issues caused by the high irreversible capacity and low ICE at the first cycle. For example, the poor electrochemical performance caused by the low ICE of Si-based anodes was improved by introducing additional Li + (or pre-lithiation) in a Si-composite anode; see [61, 62] where improvement in the electrochemical performance of the Si anode in a full cell configuration was observed. In fact, pre-lithiation of the anode has been used to improve the Coulombic efficiency of Li-ion full cells at the first cycle for different anode materials; more discussion can be found in [61]. Pre-lithiation of the Co_3O_4/C composite fibers discussed in the present work could definitively improve electrochemical performance and Coulombic efficiency at the first cycle in Li-ion full cells. However, this topic is out the scope of the present work.

Summary

Centrifugally spun carbon fibers from PAN precursors were used with a facile wet coating method to produce Co_3O_4/C composite anodes for LIBs. The increase in active material concentration in the composite-fiber anode was achieved by using highly dispersed cobalt oxides/ethanol precursor solutions, and two-step heat treatment at a low carbonization temperature. The presence of the Co_3O_4 nanoparticles during heat treatment led to the incorporation of the nanoparticles into the carbon fibers through oxygen- and nitrogen-containing ligands in the carbonized PAN fibers. This resulted in the incorporation of cobalt oxides and some metallic cobalt into the carbon backbone by nitrogen bonding. This method of fiber-composite processing allowed for the ease of production of coated polymer fibers. The difficulties associated with the centrifugal spinning of high viscosity solutions containing metallic (active material) nanoparticles were circumvented by using the proposed wet coating process, as desired high contents of active materials coated on PAN fibers were achieved. The coating method presented in this work can be used to develop both unique structures and combinations of different active materials. Coated carbon fibers yielded higher capacity with increased cobalt oxide concentration from 0 to 70 wt%. The CCF composite anodes outperformed carbon fibers at a constant current density of 100 and 200 mA g^{-1} and showed a good capacity retention after 100 cycles. Nevertheless, to design more efficient composite-fiber anodes, the problem of the large SEI must be addressed. Further research needs to be conducted to understand the carbon-fiber surface characteristics such as defects or polar group composition, and how those can be used to result in a more stable SEI formation at the fiber-anode electrolyte interface.

Funding

The authors gratefully acknowledge the support received by NSF PREM award under Grant No. DMR-1523577: UTRGV-UMN Partnership for Fostering Innovation by Bridging Excellence in Research and Student Success. The Department of Chemistry at the University of Texas Rio Grande Valley is grateful for the generous support provided by a

Departmental Grant from the Robert A. Welch Foundation (Grant No. BX-0048). Part of this work was carried out in the College of Science and Engineering Characterization Facility, University of Minnesota, which has received capital equipment funding from the NSF through the UMN MRSEC program under Award Number DMR-2011401.

Declarations

Conflict of interest The authors declare that they have no conflict of interest.

References

[1] Agubra VA, De la Garza D, Gallegos L, Alcoutlabi M (2016) ForceSpinning of polyacrylonitrile for mass production of lithium-ion battery separators. J Appl Polym Sci. https://doi.org/10.1002/app.42847

[2] Chavez RO, Lodge TP, Alcoutlabi M (2021) Recent developments in centrifugally spun composite fibers and their performance as anode materials for lithium-ion and sodium-ion batteries. Mater Sci Eng B 266:115024

[3] Chavez RO, Lodge TP, Huitron J, Chipara M, Alcoutlabi M (2021) Centrifugally spun carbon fibers prepared from aqueous poly (vinylpyrrolidone) solutions as binder-free anodes in lithium-ion batteries. J Appl Polym Sci 138(18):50396

[4] Liu L, Yin Y-X, Li J-Y, Li N-W, Zeng X-X, Ye H, Guo Y-G, Wan L-J (2017) Free-standing hollow carbon fibers as high-capacity containers for stable lithium metal anodes. Joule 1(3):563–575

[5] Ji L, Lin Z, Alcoutlabi M, Zhang X (2011) Recent developments in nanostructured anode materials for rechargeable lithium-ion batteries. Energ Environ Sci 4(8):2682–2699

[6] Campos H, Ayala J, Valdes C (2018) The use of Fe3O4/carbon composite fibers as anode materials in lithium ion batteries. MOJ Poly Sci 2(2):44–46

[7] Kim C, Yang KS, Kojima M, Yoshida K, Kim YJ, Kim YA, Endo M (2006) Fabrication of electrospinning-derived carbon nanofiber webs for the anode material of lithium-ion secondary batteries. Adv Func Mater 16(18):2393–2397

[8] Valdez A, Villarreal J, Zuniga L, Alcoutlabi M (2018) MoS2 and MoO2 loaded carbon microfibers as anode materials for lithium-ion and sodium-ion batteries. ECS Trans 85(13):357–368

[9] Zuniga L, Gonzalez G, Orrostieta Chavez R, Myers JC, Lodge TP, Alcoutlabi M (2019) Centrifugally spun α-Fe2O3/TiO2/carbon composite fibers as anode materials for lithium-ion batteries. Appl Sci 9(19):4032

[10] Calisir MD, Kilic A (2020) A comparative study on SiO2 nanofiber production via two novel non-electrospinning methods: Centrifugal spinning vs solution blowing. Mater Lett 258:126751

[11] Lukasova V, Buzgo M, Vocetkova K, Sovkova V, Doupnik M, Himawan E, Staffa A, Sedlacek R, Chlup H, Rustichelli F, Amler E, Rampichova M (2019) Needleless electrospun and centrifugal spun poly-epsilon-caprolactone scaffolds as a carrier for platelets in tissue engineering applications: a comparative study with hMSCs. Mat Sci Eng C-Mater 97:567–575

[12] De la Garza D, De Santiago F, Materon L, Chipara M, Alcoutlabi M (2019) Fabrication and characterization of centrifugally spun poly (acrylic acid) nanofibers. J Appl Polym Sci 136(19):47480

[13] Hasan MT, Gonzalez R, Chipara M, Materon L, Parsons J, Alcoutlabi M (2021) Antibacterial activities of centrifugally spun polyethylene oxide/silver composite nanofibers. Polym Adv Technol 32(6):2327–2338

[14] Tang K, Yu Y, Mu X, van Aken PA, Maier J (2013) Multichannel hollow TiO2 nanofibers fabricated by single-nozzle electrospinning and their application for fast lithium storage. Electrochem Commun 28:54–57

[15] Fang S, Bresser D, Passerini S (2020) Transition metal oxide anodes for electrochemical energy storage in lithium-and sodium-ion batteries. Adv Energ Mater 10(1):1902485

[16] Goriparti S, Miele E, De Angelis F, Di Fabrizio E, Zaccaria RP, Capiglia C (2014) Review on recent progress of nanostructured anode materials for Li-ion batteries. J Power Sources 257:421–443

[17] Liu YH, Xue JS, Zheng T, Dahn JR (1996) Mechanism of lithium insertion in hard carbons prepared by pyrolysis of epoxy resins. Carbon 34(2):193–200

[18] Ji L, Toprakci O, Alcoutlabi M, Yao Y, Li Y, Zhang S, Guo B, Lin Z, Zhang X (2012) α-Fe2O3 nanoparticle-loaded carbon nanofibers as stable and high-capacity anodes for rechargeable lithium-ion batteries. ACS Appl Mater Interfaces 4(5):2672–2679

[19] Wongittharom N, Wang CH, Wang YC, Fey GTK, Li HY, Wu TY, Lee TC, Chang JK (2014) Charge-storage performance of Li/LiFePO4 cells with additive-incorporated ionic liquid electrolytes at various temperatures. J Power Sources 260:268–275

[20] Yoon T, Chae C, Sun Y-K, Zhao X, Kung HH, Lee JK (2011) Bottom-up in situ formation of Fe 3 O 4 nanocrystals in a porous carbon foam for lithium-ion battery anodes. J Mater Chem 21(43):17325–17330

[21] Akia M, Salinas N, Luna S, Medina E, Valdez A, Lopez J, Ayala J, Alcoutlabi M, Lozano K (2019) In situ synthesis of Fe 3 O 4-reinforced carbon fiber composites as anodes in

lithium-ion batteries. J Mater Sci 54(21):13479–13490. https://doi.org/10.1007/s10853-019-03717-z

[22] Osmieri L (2019) Transition metal–nitrogen–carbon (M–N–C) catalysts for oxygen reduction reaction. Insights on synthesis and performance in polymer electrolyte fuel cells. Chem Eng 3(1):16

[23] Drew C, Wang X, Bruno FF, Samuelson LA, Kumar J (2005) Electrospun polymer nanofibers coated with metal oxides by liquid phase deposition. Compos Interfaces 11(8–9):711–724

[24] Shenashen MA, Hassen D, El-Safty SA, Isago H, Elmarakbi A, Yamaguchi H (2017) Axially oriented tubercle vein and X-crossed sheet of N-Co3O4@ C hierarchical mesoarchitectures as potential heterogeneous catalysts for methanol oxidation reaction. Chem Eng J 313:83–98

[25] Pollack B, Holmberg S, George D, Tran I, Madou M, Ghazinejad M (2017) Nitrogen-rich polyacrylonitrile-based graphitic carbons for hydrogen peroxide sensing. Sensors 17(10):2407

[26] Gu F, Li C, Hu Y, Zhang L (2007) Synthesis and optical characterization of Co3O4 nanocrystals. J Cryst Growth 304(2):369–373

[27] Teng Y, Yamamoto S, Kusano Y, Azuma M, Shimakawa Y (2010) One-pot hydrothermal synthesis of uniformly cubic Co3O4 nanocrystals. Mater Lett 64(3):239–242

[28] Liu SW, Zhu JJ, Mastai Y, Felner I, Gedanken A (2000) Preparation and characteristics of carbon nanotubes filled with cobalt. Chem Mater 12(8):2205–2211

[29] Sasaki S, Fujino K, Takéuchi Y (1979) X-ray determination of electron-density distributions in oxides, MgO, MnO, CoO, and NiO, and atomic scattering factors of their constituent atoms. Proc Jpn Acad Ser B 55(2):43–48

[30] Makkonen RJ (1962) Crystallographic and magnetic properties of solid solutions of CoCo 2 O 4 and CoCr 2 O 4. Suom Kemistil A 35:230

[31] Pindar S, Dhawan N (2019) Carbothermal reduction of spent mobile phones batteries for the recovery of lithium, cobalt, and manganese values. JOM 71(12):4483–4491

[32] Yao S, Guo R, Xie F, Wu Z, Gao K, Zhang C, Shen X, Li T, Qin S (2020) Electrospun three-dimensional cobalt decorated nitrogen doped carbon nanofibers network as free-standing electrode for lithium/sulfur batteries. Electrochim Acta 337:135765

[33] Cai N, Chen M, Liu M, Wang J, Shen L, Wang J, Feng X, Yu F (2019) Meso-microporous carbon nanofibers with in-situ embedded Co nanoparticles for catalytic oxidization of azo dyes. J Mol Liq 289:111060

[34] Dehghan R, Hansen TW, Wagner JB, Holmen A, Rytter E, Borg O, Walmsley JC (2011) In-situ reduction of promoted cobalt oxide supported on alumina by environmental transmission electron microscopy. Catal Lett 141(6):754–761

[35] Wang H, Chen C, Zhang Y, Peng L, Ma S, Yang T, Guo H, Zhang Z, Sheng Su D, Zhang J (2015) In situ oxidation of carbon-encapsulated cobalt nanocapsules creates highly active cobalt oxide catalysts for hydrocarbon combustion. Nat Commun 6(1):1-6

[36] Wang L, Zheng YL, Wang XH, Chen SH, Xu FG, Zuo L, Wu JL, Sun LL, Li Z, Hou HQ, Songt YH (2014) Nitrogen-doped porous carbon/co3o4 nanocomposites as anode materials for lithium-ion batteries. Acs Appl Mater Inter 6(10):7117–7125

[37] Dominguez M, Taboada E, Idriss H, Molins E, Llorca J (2010) Fast and efficient hydrogen generation catalyzed by cobalt talc nanolayers dispersed in silica aerogel. J Mater Chem 20(23):4875–4883

[38] Baek GY, Lee HS, Jung JM, Hwang IT, Shin J, Jung CH, Choi JH (2018) Preparation of conductive carbon films from polyacrylonitrile/graphene oxide composite films by thermal treatment. J Ind Eng Chem 58:87–91

[39] Zhang L, Hu P, Zhao X, Tian R, Zou R, Xia D (2011) Controllable synthesis of core–shell Co@ CoO nanocomposites with a superior performance as an anode material for lithium-ion batteries. J Mater Chem 21(45):18279–18283

[40] Yao W, Chen J, Cheng H (2011) Platelike CoO/carbon nanofiber composite electrode with improved electrochemical performance for lithium ion batteries. J Solid State Electrochem 15(1):183–188

[41] Do J-S, Weng C-H (2005) Preparation and characterization of CoO used as anodic material of lithium battery. J Power Sources 146(1–2):482–486

[42] Laruelle S, Grugeon S, Poizot P, Dolle M, Dupont L, Tarascon J (2002) On the origin of the extra electrochemical capacity displayed by MO/Li cells at low potential. J Electrochem Soc 149(5):A627–A634

[43] Wang G, Chen Y, Konstantinov K, Lindsay M, Liu H, Dou S (2002) Investigation of cobalt oxides as anode materials for Li-ion batteries. J Power Sources 109(1):142–147

[44] Kim T, Choi W, Shin H-C, Choi J-Y, Kim JM, Park M-S, Yoon W-S (2020) Applications of voltammetry in lithium ion battery research. J Electrochem Sci Technol 11(1):14–25

[45] Rai AK, Anh LT, Gim J, Kim J (2013) One-step synthesis of CoO anode material for rechargeable lithium-ion batteries. Ceram Int 39(8):9325–9330

[46] Rothermel S, Meister P, Schmuelling G, Fromm O, Meyer HW, Nowak S, Winter M, Placke T (2014) Dual-graphite cells based on the reversible intercalation of bis(trifluoromethanesulfonyl)imide anions from an ionic liquid electrolyte. Energ Environ Sci 7(10):3412–3423

[47] Wu J, Lau WM, Geng DS (2017) Recent progress in cobalt-based compounds as high-performance anode materials for lithium ion batteries. Rare Met 36(5):307–320

[48] Qi W, Shapter JG, Wu Q, Yin T, Gao G, Cui DX (2017) Nanostructured anode materials for lithium-ion batteries: principle, recent progress and future perspectives. J Mater Chem A 5(37):19521–19540

[49] Yang S, Song H, Chen X (2006) Electrochemical performance of expanded mesocarbon microbeads as anode material for lithium-ion batteries. Electrochem Commun 8(1):137–142

[50] Fu Y, Wei Q, Wang X, Shu H, Yang X, Sun S (2015) Porous hollow α-Fe 2 O 3@ TiO 2 core–shell nanospheres for superior lithium/sodium storage capability. J Mater Chem A 3(26):13807–13818

[51] Schmitt J, Maheshwari A, Heck M, Lux S, Vetter M (2017) Impedance change and capacity fade of lithium nickel manganese cobalt oxide-based batteries during calendar aging. J Power Sources 353:183–194

[52] Forney MW, Ganter MJ, Staub JW, Ridgley RD, Landi BJ (2013) Prelithiation of silicon-carbon nanotube anodes for lithium ion batteries by stabilized lithium metal powder (SLMP). Nano Lett 13(9):4158–4163

[53] Lee BS (2020) A review of recent advancements in electrospun anode materials to improve rechargeable lithium battery performance. Polymers 12(9):2035

[54] Liberale F, Fiore M, Ruffo R, Bernasconi R, Shiratori S, Magagnin L (2020) Red phosphorus decorated electrospun carbon anodes for high efficiency lithium ion batteries. Sci Rep 10(1):1–11

[55] He HN, Sun D, Tang YG, Wang HY, Shao MH (2019) Understanding and improving the initial coulombic efficiency of high-capacity anode materials for practical sodium ion batteries. Energ Storage Mater 23:233–251

[56] Park S, Jeong SY, Lee TK, Park MW, Lim HY, Sung J, Cho J, Kwak SK, Hong SY, Choi NS (2021) Replacing conventional battery electrolyte additives with dioxolone derivatives for high-energy-density lithium-ion batteries. Nat Commun 12(1):1–12

[57] Choudhury S, Archer LA (2016) Lithium fluoride additives for stable cycling of lithium batteries at high current densities. Adv Electron Mater 2(2):1500246

[58] Tornheim A, He MN, Su CC, Zhang ZC (2017) The role of additives in improving performance in high voltage lithium-ion batteries with potentiostatic holds. J Electrochem Soc 164(1):A6366–A6372

[59] Aravindan V, Arun N, Shubha N, Sundaramurthy J, Madhavi S (2016) Overlithiated Li1+xNi0.5Mn1.5O4 in all one dimensional architecture with conversion type alpha-Fe2O3: a new approach to eliminate irreversible capacity loss. Electrochim Acta 215:647–651

[60] Hassoun J, Croce F, Hong I, Scrosati B (2011) Lithium-iron battery: Fe2O3 anode versus LiFePO4 cathode. Electrochem Commun 13(3):228–231

[61] Meng QH, Li G, Yue JP, Xu Q, Yin YX, Guo YG (2019) High-performance lithiated SiOx anode obtained by a controllable and efficient prelithiation strategy. Acs Appl Mater Inter 11(35):32062–32068

[62] Chen T, Wu J, Zhang QL, Su X (2017) Recent advancement of SiOx, based anodes for lithium-ion batteries. J Power Sources 363:126–144